A Ray Tracing Algorithm for Microcellular Wideband Propagation Modelling

G.E.Athanasiadou, A.R.Nix and J.P.McGeehan

Centre for Communications Research,
University of Bristol, Queen's Building, University Walk, Bristol BS8 1TR, UK.
Fax: +44 (0)117 9255265, E-mail: G.Athanasiadou@bristol.ac.uk

Abstract: **In this paper a 3-D 'image-based' ray tracing algorithm for microcellular environments is presented. The model is capable of predicting wideband as well as narrowband propagation information. To demonstrate the viability of this approach, predictions are generated using a two dimensional building database for the centre of Bristol. These results are then compared with practical wideband measurements.**

I. INTRODUCTION

Over the last decade the mobile communications industry has experienced phenomenal growth. As the number of communication devices continues to increase, the trend towards high capacity microcellular communication networks will grow. However, unlike previous large cell scenarios, statistical propagation models no longer provide acceptable results [1]. Due to the site specific nature of these microcellular environments, propagation models are now required to take into account the exact position, orientation and electrical properties of individual buildings. These new simulation tools will enable researchers and designers to accurately predict the performance of wireless systems under a wide range of conditions. As cell sizes reduce, the need to accurately plan basestation locations will become critical due to a need to minimise infrastructure costs.

Ray tracing produces deterministic channel models that operate by processing user-defined environments. It represents the high frequency limit of the exact solution for electromagnetic fields and gives approximate results when the exact solution cannot be found. In recent years, many authors have investigated the application of ray tracing to predict the amplitudes, time delays and arrival angles of the various multipath components arriving at the receiver [2-8]. While many of these models are academically interesting, the raw processing time required to generate a result can seriously affect their application. Alternatively, since the majority of ray models require a simplified database, this prevents their use in more practical environments.

In this paper a ray tracing algorithm is presented that allows the rapid generation of complex channel impulse response characteristics for any given location of transmitter and receiver. The model makes full use of reflection, transmission and diffraction and, with sufficient memory, can evaluate scenarios incorporating many thousands of objects.

Previous models have been 2D or 3D in nature, in this paper a hybrid technique is presented where the object database is held in two dimensions but the ray-tracing engine operates in three dimensions. This hybrid analysis allows factors such as polarisation and 3D antenna patterns to be fully considered in the model. In this paper modelled and measured results are presented for a location in the centre of Bristol.

II. MODELLING APPROACH

THE IMAGE TECHNIQUE: Ray tracing represents electromagnetic waves as rays which are generated and launched in three dimensional space from the transmitter location. There are many types of ray-tracing techniques reported in the literature [2-8]. In this paper a technique based on the electromagnetic theory of images has been developed [3]. Rather than using a 'ray launching' approach where rays are sent out at various angles and their path traced until a certain power threshold is reached, the technique adopted here considers all walls and obstacles as potential reflectors and evaluates the location of their transmitter images. This imaging technique works by conceptually generating an image table for each transmitter location. This process is implemented by considering all the various wall reflection, transmission and diffraction permutations that are possible in a given area. This image information is then stored in an array and used to compute the channel characteristics at each receiver location. The use of such an image map dramatically improves the operating speed of the algorithm since repetitive calculations no longer have to be performed.

THE PROPAGATION MODEL: In a wireless communications system, the signal arriving at the receiver consists of several multipath components, each of which is the result of the interaction of the transmitted waves with the surrounding environment. The equation used to describe the mobile channel was first proposed by Turin [11] and

0-7803-2742-X/95 $4.00

takes the form of a bandlimited complex impulse response $h(t)$ given by:

$$h(t) = \sum_{n=1}^{N} A_n \delta(t - \tau_n) e^{-j\theta_n} \qquad (1)$$

Here, the transmitted impulse is mathematically described by a Dirac function and the received signal $h(t)$ formed from the vector addition of a number of time delayed rays, each represented by an attenuated and phase-shifted version of the original Dirac waveform. For each ray, the model computes the amplitude A_n, arrival time τ_n and the arrival phase θ_n.

Reflected and transmitted rays are evaluated through the use of geometrical optics while diffracted rays are calculated using the geometrical theory of diffraction [12-14]. According to the objects encountered by the i^{th} ray, its complex received field amplitude E_i(V/m) is given by:

$$E_i = E_0 f_{ti} f_{ri} \left\{ \prod_j R_j \prod_k T_k \prod_l A_l(s',s) D_l \right\} \frac{e^{-jkd}}{d}. \qquad (2)$$

where E_0 represents the reference field strength (V/m), f_{ti} and f_{ri} the transmitting and the receiving antenna field radiation patterns in the direction of the ray, R_j the reflection coefficient for the j^{th} reflector, T_k the wall transmission coefficient for the k^{th} transmission, D_l the diffraction coefficient for the l^{th} diffracting wedge and e^{-jkd} the propagation phase factor due to the path length d ($k = 2\pi / \lambda$). The diffraction coefficients are also multiplied by a spatial attenuation function $A_l(s',s)$ which finds the correct multiplicative diffraction coefficient given the $1/d$ dependence in the last term. All coefficients are functions of the angle of incidence and the object characteristics. In [3] a full explanation of the individual transmission, reflection and diffraction calculations can be found. The above approach is used to model the complex impulse response with no loss of phase information.

III. Modelling Assumptions

In urban areas, the signal is normally confined by local structures. The model described in this paper has been optimised for use in microcellular environments. The base station and the mobiles are assumed to remain below roof top height, using this assumption it is reasonable to model buildings as infinitely tall. Although the building database is two dimensional, the model generates a 3D environment by specifying the transmitter and receiver heights. For each path found in the image tree, an additional ray is created corresponding to its ground reflection (figure 1). Since the transmitter and receiver are stored using 3-D co-ordinates, the plane of the ray can be calculated and all reflections, transmissions and diffractions computed using 3-D vector mathematics.

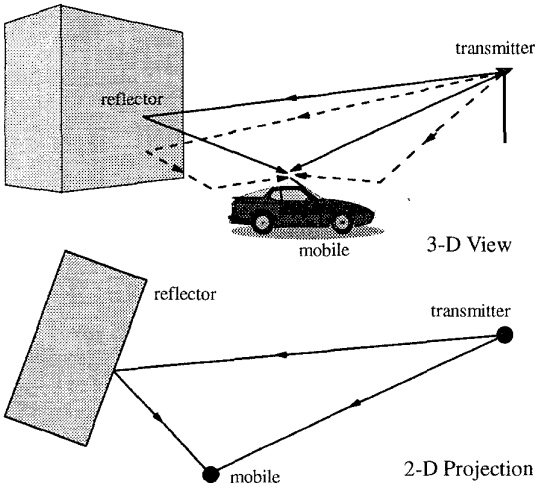

Figure. 1: 2D/3D hybrid analysis

To make the algorithm as realistic as possible, each wall is characterised by its permittivity, conductivity and thickness. Wall thickness is required in the calculation of the reflected and transmitted field strengths [3]. The reflection and transmission coefficients are evaluated as a function of incident angle for a range of different wall materials. The wall parameters can be edited individually for each object or a single bulk parameter can be applied to the map. Walls are assumed to be perpendicular to the ground but not necessarily to each other and the ground is assumed flat.

To ensure as generic a model as possible, wall transmission and corner diffraction are fully supported even for onward propagating cases, i.e. each wall transmission or corner diffraction can undergo subsequent diffractions, reflections and transmissions. The maximum number of allowable transmissions, reflections and diffractions for each path is defined by the user and has no restriction. For microcellular studies, wall transmission is often ignored, however for determining in-building coverage this process needs to be modelled.

For ray tracing to be used in practical situations the model must be capable of importing standard building databases. In this paper the Bristol building data was extracted from the UK Ordnance survey 'Landline' database. The map was then pre-processed to remove any redundant information and diffraction corners were automatically added.

The speed of the model is obviously a function of the number of objects in the building database and the number of reflections, transmissions and diffractions permitted in the ray engine. Due to the complex nature of the

microcellular environment, large amounts of memory can be required to store pre-processed 'image maps'. It is the generation of such image maps that greatly enhance the speed of the model. Due to these restrictions, the model have been written to operate efficiently on UNIX workstations. Currently, maps incorporating several thousand objects have been successfully studied with ray tracing to individual points taking a matter of seconds on a HP735 workstation*.

IV. Model Validation

The most effective way to evaluate the accuracy of a propagation model is to compare its results with measurements taken in a real environment. The impulse response obtained from a ray tracing model corresponds to measurements made with infinite bandwidth (i.e. each received ray corresponding to a perfect impulse in the time domain). To be able to compare simulated results with actual measurements, the impulse response must be convolved with the autocorrelation of the PN-sequence used in the measurement system. Figure 2 shows the autocorrelation of the PN sequence used in the channel sounder (a 511 bit sequence was used).

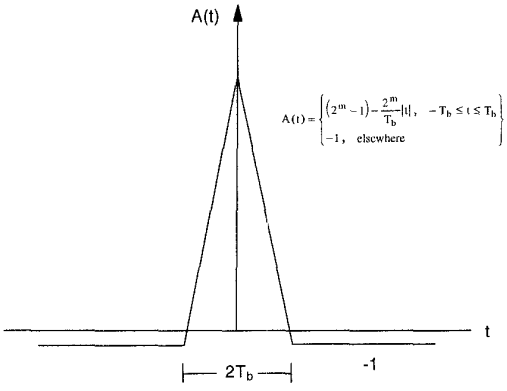

Figure 2: PN Sequence Autocorrelation

The output $P(\tau)$, represents a model of the power delay profile as seen at the resolution of the measurement hardware. This output can be calculated as shown in equation 3, where *A(t)* represents the amplitude of the autocorrelation function shown above.

$$P(\tau)=\left|\sum_{n=-\infty}^{\infty} h(\tau-t_n)A(t_n)\right|^2 \qquad (3)$$

Figure 3 illustrates the microcellular map used in this modelling process. The diagram shows a 350m by 400m area of central Bristol including the University of Bristol's Engineering Building, Park Street and College Green. The transmitter was located in the College Green area and measurements taken along the test route indicated. The simulation and measurement results were taken at a frequency of 1.834 GHz. The heights of the transmitting and the receiving dipole antennas were 3m and 1.5m respectively and the transmitted power was 20dBm.

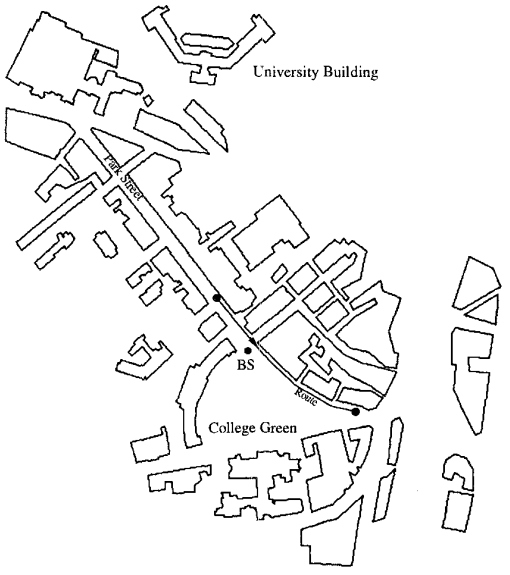

Figure 3: Microcellular Map & Test Route

The buildings shown in figure 3 above were modelled using a single set of electrical properties (ε_r=5, σ=0.05 Sm^{-1}). The walls were assumed smooth and to have a thickness of 0.4m. For the results shown in this paper, all rays were traced up to seven orders of reflection and one order of diffraction. Figure 4 shows a typical power delay profile produced from the propagation model. In addition to showing individual rays at infinite resolution, the graph also shows the simulated impulse response taking into account the resolution of the 8 MHz channel sounder (see equation 3). Two sets of measurements are also shown at this point, the second set being taken several minutes later.

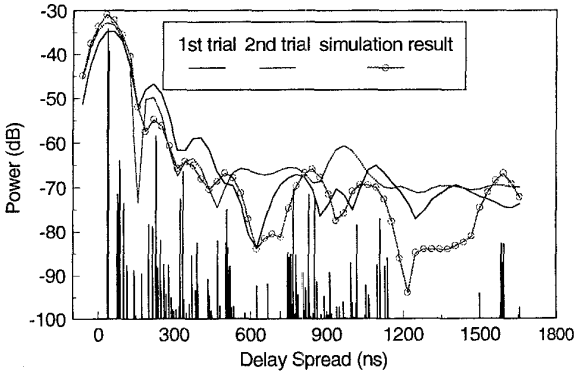

Figure 4: Measured vs Modelled Delay Profile

* This particular version was produced by Tony Au as part of a Research contract funded by the University of Bristol.

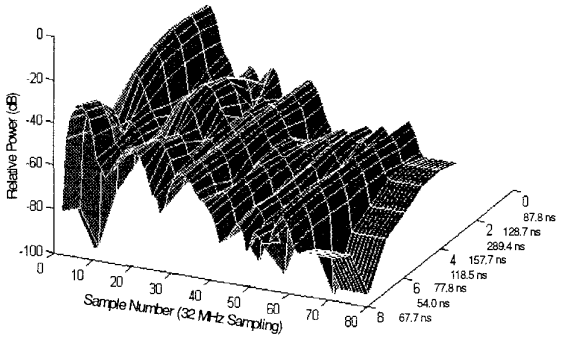

Figure 5: 'Finite Bandwidth' Profile Variation

In practice, the use of a finite bandwidth in the channel sounder introduces some variability into the measured delay profile. For example, using an 8 MHz PN-based sounder, the chip duration lasts 125 ns. This limited time resolution results in the multipath addition of rays arriving at similar times. Hence, the resulting power delay profile at any time τ is generated from the vector summation of all multipath components within the time resolution of the sounder. The actual profile shape (and hence the rms delay spread) is therefore a function of the phase of many individual arriving rays. This phenomenon is shown graphically in figure 5 where an identical modelled profile at infinite resolution has been processed to an 8 MHz bandwidth at half wavelength intervals.

Figure 5 shows that the resulting 'finite bandwidth' profiles differ significantly in both their shape and rms delay spread. The rms delay spreads vary from as low as 54 ns to as high as 289 ns. For comparison, the original infinite bandwidth profile has an rms delay spread of 90 ns, the mean simulated rms delay spread was 122 ns while the measured value was 125 ns (this level of agreement is not seen at all points in the simulated route). It is clear from these observations that since this kind of propagation model cannot accurately predict arrival phase [3], for a single individual point it will be unable to achieve agreement in either the measured profile shape or the value of rms delay spread. To achieve agreement between measured and modelled results, the average rms delay spread for a given area must be calculated.

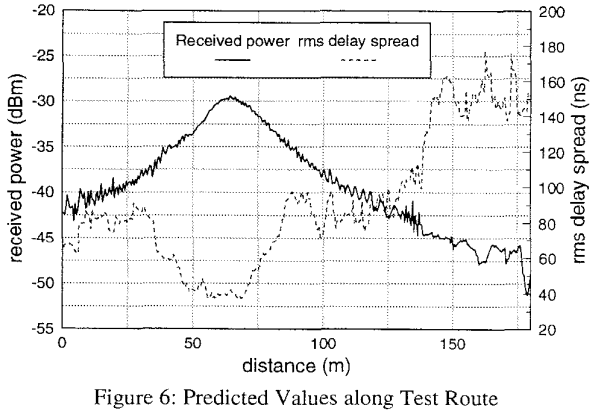

Figure 6: Predicted Values along Test Route

Figure 6 shows the predicted average signal power and rms delay spread for a 180m route passing through the College Green area of central Bristol (see figure 3). Power can be seen to peak at around 70 metres into the route, this corresponds to the user passing close to the transmitting basestation. At this location, the rms delay spread is at its minimum value since a strong line-of-sight is received.

Figure 7 shows two sets of measured rms delay spread results for the route indicated in figure 3 (a 20 dB power window was used in these calculations). The second set of measurements was taken at the same location several minutes later using the same hardware. Each set of measured delay spreads show considerable variability from point to point and as described previously this arises due to the finite bandwidth used by the sounder. Due to time variations in the channel, there are several discrepancies between these two sets of measurements. This highlights an important point, it is not reasonable to expect these types of model to produce agreements better than that obtained between identical measurements in the same location.

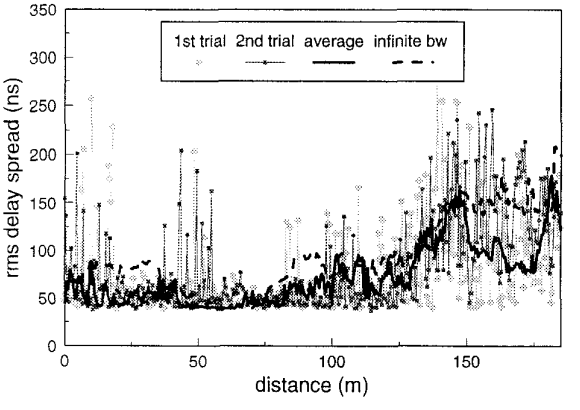

Figure 7: Measured vs Simulated RMS Delay Spread

Most validation processes assume the measured data to be 'correct' and attribute all error to the modelling process. In reality, there would be significant variations in measured data taken at the same location at slightly different times. It is perhaps more useful to compare the error between modelled data and at least two sets of practical measurements. The modelled error relative to the measured error would then indicate how well the model can produce a set of valid results. Figure 7 also shows the modelled infinite bandwidth rms delay spread and the average rms delay spread calculated from 16 profiles spaced at half wavelength intervals. As expected, at infinite resolution the modelled delay spread varies smoothly, it is encouraging to

note that the measured 'finite bandwidth' data varies above and below the model's average predicted value.

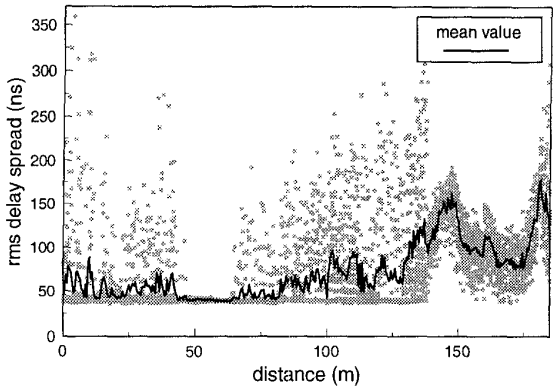

Figure 8: Average vs Instantaneous Predicted Dispersion

Figure 8 shows the modelled instantaneous rms delay spread variations assuming the channel sounder response defined earlier. In a manner similar to the measured results in figure 7, these plots show significant variations in rms delay spread. The actual variation is a function of the receiver bandwidth. For each location, the 16 instantaneous values have been processed to generate the more familiar average rms delay spread (solid line).

V. Conclusions

The paper has presented a site specific urban propagation model suitable for microcellular environments. This model has then been applied to a detailed scenario in the centre of Bristol. Complete Complex Impulse Response (CIR) information has been predicted at individual points and the data processed to generate specific information such as average signal power and rms delay spread. The work has shown that a degree of care must be taken when comparing predicted and measured results. Practical rms delay spread measurements are a function of multipath phase and hence vary significantly at distances separated by fractions of a wavelength. In this paper, the rms delay spread at 'infinite resolution' has been compared with two sets of wideband measurements. Although on a point by point basis there was significant variation between the two sets of data, the average modelled values appear to agree well with the trend in the measured results.

Acknowledgements

G.E. Athanasiadou wishes to thank BNR Europe Ltd. for the financial support of this work. The authors would also like to thank Dr M.C.Lawton and Dr J.S.Hilton for the useful conversations and encouragement during the development of these models. The authors acknowledge the support of their colleagues in the Centre for Communications Research, especially Mr T.Au for the use of his database conversion utilities. We thank Dr M.A.Beach and Mr C.M.Simmonds for the propagation measurements used in this paper, and the CEC RACE PLATON project (R2007) under which this equipment was initially constructed.

References

[1] M.J.Mehler, "The microcell propagation challenge", *IEE Colloquium on "Microcellular propagation modelling"*, Nov. 1992

[2] J.W.McKnown and R.L.Hamilton, "Ray-tracing as a design tool for radio networks", *IEEE Networks Mag.*, pp. 21-26, Nov. 1991.

[3] M.C.Lawton, J.P.McGeehan, "The application of a deterministic ray launching algorithm for the prediction of radio channel characteristics in small-cell environments", *IEEE Trans. on Veh. Technol.*, vol. 43, no. 4, Nov. 1994.

[4] T.Kurner, D.J.Cichon, W.Wiesbeck, "Concepts and results for 3-D digital terrain-based wave propagation models: an overview", IEEE Journal on Sel. Areas in Comm., pp. 1002-1012, Sept.1993.

[5] G. Yang, K. Pahlavan, J.F. Lee, A.J. Dagen, J. Vancraeynest, "Prediction of Radio Wave Propagation in Four Bocks of New York City Using 3-D Ray Tracing", *IEEE PIMRC 1994*, A3.2, vol. I, pp. 263-267.

[6] K.R.Schaubach, N.J.Davis IV, "Microcellular radio-channel propagation prediction", *IEEE Antennas and Propag. Mag.*, pp.25-34, August 1994.

[7] S.Y.Seidel, T.S.Rappaport, "Site- specific propagation prediction for wireless in-building personal communication system design", *IEEE Trans. Veh. Technol.*, vol. 43, no 4, November 1994.

[8] K.J.Gladstone and J.P.McGeehan, "Computer simulation of multipath fading in the land mobile radio environment", *IEE Proc.*, vol. 27, Pt.G., pp.323-330, no. 6, Dec.1980.

[9] M.C. Lawton, J.P.McGeehan, "The application of GTD and ray launching techniques to channel modelling for cordless radio systems", *Proceedings of the 1992 IEEE Veh. Tech. Society Conf.*, Denver, pp. 125-130, May 1992.

[10]G.E.Athanasiadou, A.R.Nix, J.P.McGeehan, "A ray tracing algorithm for microcellular and indoor propagation modelling", to be published in *ICAP '95*.

[11]G.L.Turin et.al. "A statistical model for urban multipath propagation", *IEEE Trans. Veh. Technol.*, vol. VT-21, pp. 1-9, Feb. 1972.

[12]J.B.Keller, "Geometrical Theory of Diffraction", *J. Opt. Soc. Amer.*, vol. 52, pp. 116-130, February 1962

[13]R.G.Kouyoumjian and P.H.Pathak, "A uniform geometric theory of diffraction for an edge on a perfectly conducting surface", *Proc. IEEE*, vol. 62, no. 11, pp. 1448-1461, Nov. 1974.

[14]R.Luebbers, "Finite conductivity uniform GTD versus knife edge diffraction in prediction of propagation path loss", IEEE Trans. Anten. Propag., vol. AP32, no. 1, January 1984.